Original Research Paper

IJES *Iranian Journal of Earth Sciences*
Vol. 15, No. 4, 2023, 248-263.
DOI:10.30495/ijes.2023.1936911.1639

The petrology and geochemistry of Sorkheh-Dizaj intrusive rocks in northern Zanjan and its effects on recovery of LREE from tailingby digestion-water leaching processes, Iran

Ahmad Adib*[1], Esmaeil Rahimi[1]

1. Department of Petroleum and Mining Engineering, South Tehran Branch, Islamic Azad University, Tehran, Iran.

Received 18 December 2022; accepted 1 October 2023

Abstract

Magnetite-apatite mineralization in Tarom Mountains at the western part of Alborz-Azerbaijan belt originated from quartz monzonite magma and belongs to high K calc-alkaline, showing a post-collision tectonic environment. The negative trend from LREEs to HREEs is consistent with the spider pattern of the subduction areas. In this article, the recovery of the rare-earth elements (REEs) from apatite flotation concentrate by acid leaching and digestion-water leaching were studied. The total amount of LREEs in the tailings sample is between 1500 - 2600 ppm. The most frequent elements are Ce, La, Nd, and Y. Among them Ce is the most abundant and La is the least.. The maximum LREEs recovery with the sulfuric acid leaching was62% with experimental parameters of 12 M acid concentration, 4 h leaching time, 25℃ heat, and a liquid to solid ratio (L/S) of 1:5. under optimal parameters of (220℃), (3 h), and L/S (1:2), the digesting with sulfuric acid resulted to the recovery of La, Ce, Nd, and Y with 93.92%, 92.22%, 92.04%, and 91.00%, respectively. similarity, the best conditions at water leaching process, are the leaching time of 5 h, at 80℃, and L/S of 1:10 for La, Ce, Nd, and Y recovery are respectively 89.50%, 88.45%, 92.20%, and 94.0%.

Keywords: *Acid leaching, LREE, Morvarid Mine, Digest- water leaching.*

1. Introduction

The igneous rocks of the western Alborz-Azarbaijan zone have been formed in magmatic and back-arc tectonic positions in a post-collisional setting with calc-alkaline-potassic character (Hassanzadeh et al. 2002). According to field studies, Miocene volcanic rocks have cut late Eocene-Oligocene granitoid masses. The processes of extensive magmatic and volcanic activity in the area assuming the final closure of the Neo-Tethys in the Miocene can be attributed to the Neogene extensional phases and they are attributed to crustal thinning following continental collision. The Morvarid granite is enriched in discordant elements, specifically, K, Rb, Sr, Cs, U, and Pb, and poor in high field strength (HFS) elements, particularly, Zr, Ti, and Y. Such elemental specifications revealing the arc-related magmatism (Thirlwall et al. 1994).U-Th/He apatite isotopic data in Mahneshan area of Zanjan province indicated the Miocene continental collision in Iran (Stockli et al. 2004). In the Zanjan area, magnetite-apatite mineralization originated from quartz monzonite magma related with the closure of the Neo-Tethys and formed the Sorkheh Dizaj-Morvarid zone Iron Ore Deposits in the SE of Zanjan.

Based on the geochemistry of the Morvarid magnetite ore and associated rocks, and also the fluid inclusion studies of the apatite and quartz, it is suggested, that the post magmatic hydrothermal activity relatively is the origin of the magnetite deposits, rather than the silica–iron oxide immiscibility process (Azizi et al. 2009). The Rare earth elements in syngeneic and epigenetic deposits areformed in a wide range of geodynamic positions (Jones et al. 1996), and LREEs have a higher degree of incompatibility than the HREEs, and tend to be accumulate in magmatic differentiation final products (Henderson 1984).

The REE due to their distinct spectroscopic attributes have significant role in the manufacture of main industrial supplies (Kim et al. 2009; Kim 2012). Thus, it is required to meet the new processing of REMs and to develop suitable methods for recovery, isolation and purification of the REEs.

Due to the same size of REE and calcium ions, REEs ions can easily replace calcium ions in the apatite network, accordingly, apatite is considered as a REEs contained mineral (Gupta and Krishnamurthy 2005). The general formula of apatite is Ca10 (PO4)6X2, which X is the fluorine ion with chlorine and one hydroxyl group (Preston et al. 1996). RREs minerals are often treated by physical separation and leaching. The physically separating procedure significantly increases the amount of REEs, but provided, the REEs to be mainly concentrated in a lone mineral phase such as bastnäsite (REECO3F) or monazite (REEPO4) (Chi et al. 2006).

REEs in the apatite [$Ca_{10}(PO_4)_6(OH,F,Cl)_2$] commonly occur as ionic replacements instead of calcium in its crystal lattice in the form of separate minerals. Naturally, it is probable to recover REE concentrates from Iron ore apatite. There are many methods in extraction of REEs from the ore. Leaching by acidic or alkaline reagents are the most frequently used techniques. In the digestion acid method is frequently used for the major REE in minerals such as, monazite, apatite, bastnäsite, and xenotime. In

*Corresponding author.
E-mail address (es): adib@azad.ac.ir

these techniques, sulfuric acid is added to concentrates contain REE at temperature about 200°C. Subsequently, the resulted cake is leached with water to dissolve REEs (Kim et al. 2016). Some investigations on the REE leaching showed that apatite is well leached in hydrochloric and nitric acid under normal conditions, for leaching with sulfuric acid, acid with high concentration and/or high temperature should be used(Jorjani et al. 2011; Sandström and Fredriksson 2012; Pereira and Bilal 2016; Gharib-Gorgani et al. 2017; Adib et al. 2021b; Sarem et al. 2021; Yazdi et al. 2022). However, due to the complexity of REEs metallogeny, the various processes are in practice for leaching of REE-bearing minerals. The optimal dissolution process is strongly specified the mineralogical composition of the REE ore.

In this research, investigating the geochemical properties of REEs by using nitric, sulfuric and hydrochloric acids on the dissolution of REEs in the tailings of the iron processing plant of Morvarid Mine is pursued as the main goal. Additionally, the study also describe the procedure of the digestion method using sulfuric acid and consequently by the water leaching of the iron- removed concentrate, by applying various parameters. Due to the specific spectroscopic and magnetic properties of REEs, these elements play an important role in manufacturing of permanent magnets, electronics, superconductors, and also in hydrogen storage, medical and nuclear technologies (Fig.1) (Kim and Osseo-Asare 2012).

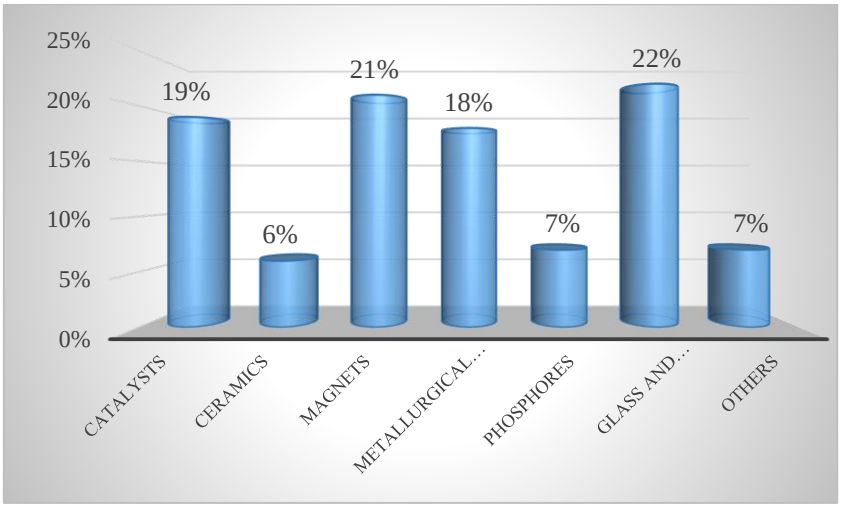

Fig 1. The Comparison of special uses of Rare earth metals (Kim and Osseo-Asare 2012)

2. Geology of Region

The tectonic happenings and magmatic phenomena represent the geological evolution of Iran (Ghasemi and Talbot 2006; Davoudian et al. 2008). The tectonics of Iran is influenced by the expansion of the Tethyan oceans. The inactive margin of the Neotethys Ocean in the late Triassic has re-emerged in the final stages, opening up the Bitlis and Zagros oceans in the middle to upper Triassic. The subduction of Neotethys, which has been active since late Jurassic, occurred in Cretaceous (Golonka 2004), in which the tectonic regime between the micro continent margins of the Arabian and Sanandaj-Sirjan has become an active convergence regime from the inactive margin in late Cretaceous (Şengör and Nataln'in 1996). The closure of Neo-Tethys Ocean and also Tarom intrusive masses resulted the generation of quartzmonzonite magma with magnetite-apatite mineralization. The deposits of Sorkheh-Dizaj, Ali Abad, Morvarid, Zaker, and Golestan Abad are typical field evidence (Fig 2).

The main intrusive masses of the area are composed of quartzmonzonite to quartz monzodiorite and the coarse crystals include plagioclase, pyroxene and a small amount of quartz. The secondary minerals of these intrusive rocks include magnetite, zircon, apatite, and a small amount of sphene.

In the geological map (Fig. 2), the rock units of the magnetite-apatite mineral zone of Sorkheh-Dizaj and the intrusive masses originated by the closure of the Neo-Tethys Ocean are displayed. Circulation of hydrothermal solutions or fluids into these intrusive masses have led to mineralogical changes including the conversion of plagioclase to clay minerals, sericite, epidote, and calcite. The Tarom region (NW Iran) comprises metallic mines and deposits, especially Cu, Fe, Pb, Zn, and REEs with hydrothermal genesis (Mokhtari et al. 2018; Baratian et al. 2018). These deposits (e.g., Morvarid and Sorkhe-Dizaj) are in Tarom metalogenic region including Fe, Cu, REEs, Au and Pb-Zn mineralization with Late Eocene magmatic and volcano sedimentary host rocks (Nabatian and Ghaderi2014). In Tarom region, Fe, Cu and REEs mineralization has hydrothermal source such as the Fe-

Cu-REEs deposits of the world (Yazdi et al. 2015; Nabatian et al. 2017).

Mineralization of the iron oxide-apatite of the region mostly occurs in the form of veins within the intrusive mass of quartz monzonite to quartz monzodiorite, and to a lesser extent within the volcanic rocks of Eocene. Mineralization follows the faults extensions. In these deposits, mineralization embraces magnetite, apatite, monazite, and to a lesser extent pyrite, chalcopyrite and bornite, and still to a lesser extent mineral, e.g., ilmenite and spinel magnetite. There are many metallic mines/deposits such as Morvarid. The major intrusive rock is quartz microdiorite/monzonite as the main host rock of metallic ores especially in Morvarid deposit (Fig 3).

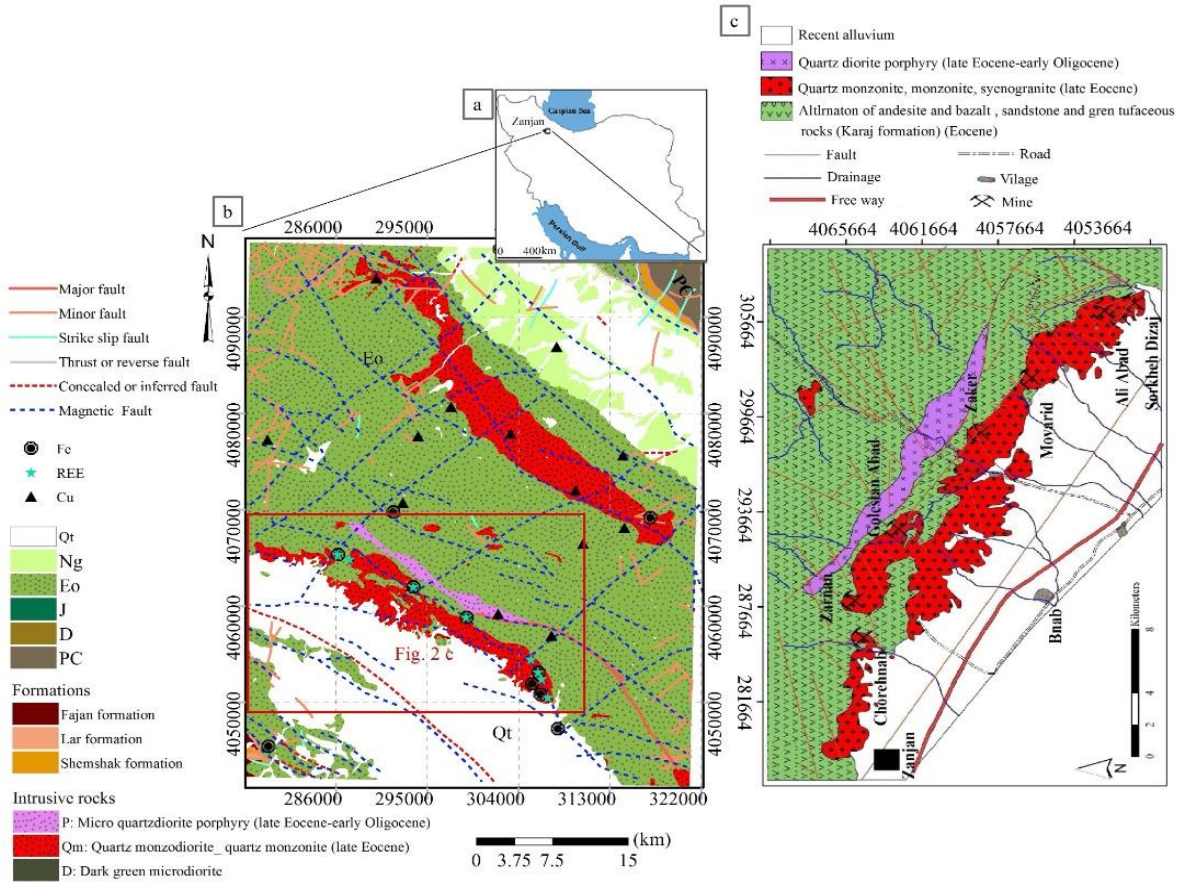

Fig 2. a. Situation of study area on global scale (Iran country) b. geological map of Tarom. Magnetic basement faults are extracted from magnetic data (Adib et al. 2021a). c.Geological map of the east of Zanjan showing the iron ore-apatite belt of the Sorkheh-Dizj mines (developed based on, Nabatian and Ghaderi 2013)

Fig 3. Mineralization of apatite iron ore within monzogranite to syenogranite and creation of economic reserve of iron and REEs in Morvarid Mine in Tarom belt of Zanjan.

3. Materials and Methods

The acid and digestion-water leaching experiments were carried out on the apatiteflotation concentrate with size dimension of d_{80}=75µm (table 1) subjecting to Sulfuric, nitric, and chloridric acids with a concentration of 95%, 65%, and 37% (Merck), respectively.

Table 1. Sketch of the Apatite flotation concentrate preparation processes

Mineralization and geochemistry of sample		
Iron tailing study		
Jaw& cone crusher and ball mill		
Low-intensity wet magnetic separation (0.2 T)		
Non-magnetic		Magnetic
Flotation of apatite		
	Apatite concentrate	
Acid leaching & digest-water leaching experiments		

3.1. Characterization of the Apatite Concentrated

The petrography, ore microscopy, XRD, Electron Micro Probe, ICP-MS, and XRF Analysis were carried out to understand the mineralogical and geochemical composition of the samples collected from the Morvarid processing plant. The equipment specifications are; inductively coupled plasma opticalemission spectrometry (ICP-OES- Perkin Elmer DRC-II quadrupole), X-ray fluorescence (Philips PW240,Netherlands), and X-ray diffraction (D/MAX 2200, Rigaku, Japan, X-ray diffractometer). Based on the results of XRF tests (Table 2), the dominant compounds of the used concentrate are SiO_2, P_2O_5, Fe_2O_3, and CaO.

Table 2.X-ray fluorescence (XRF) analysis of apatite concentrate

Chemical components	SiO_2	Al_2O_3	CaO	MgO	TiO_2	SO_3
(wt %)	27.30	9.14	8.45	6.50	3.59	0.61
Chemical components	P_2O_5	Na_2O	K2O	ZnO	CuO	MnO
(wt %)	11.45	2.17	2.13	1.1	0.1	0.1
Chemical components	CeO_2	La_2O_3	Nd_2O_3	Y_2O_3	Fe_2O_3	L.O.I
(wt %)	1.75	0.63	1.61	0.84	11.51	0.97

According to the ICP-OES results (Table 3), the apatite concentrate contains 1.74%.CeO_2, 0.65% La_2O_3, 1.62% Nd_2O_3 and 0.84 Y_2O_3). The concentrate is consist of 4.86% REEs (La, Ce, Y and Nd) and the apatite, quartz, calcite, magnetite, and plagioclase minerals.

Table 3. ICP-OES results for apatite concentrate.

Rare earth element	La_2O_3	CeO_2	Nd_2O_3	Y_2O_3	Total (wt %)
wt %	0.651	1.740	1.625	0.843	4.859

3.2. Mineralogical Studies

The apatite concentrate, were divided in three fractions (+300-150µ), (+150-75µ) and (≤75µ), for mineralogical investigation by electron-probe microanalysis (EPMA), Scanning Electron Microscope (SEM) and the analysis of some minerals were carried out by XRD methods. We have used Leo 1450 Vp Scanning Electron Microscope, electron-probe microanalysis CAMECA EPMA (SX 100 model) and Philips-Xpert Pro XRD to help identifying minerals by their composition (tables 4-5)

Table 4. The results of chemical analysis of tailing samples of the processing plant
(Oxides are reported in wt % and trace elements in ppm)

Samples	granite					granodiorite	quartz monzodiorite		
	W3	W1	Ba	Ba.E	Ba.E2	Ba.E3	W4	Ba.E4	Ba.1
SiO2	70.24	70.21	69.27	70.13	69.34	60.98	61.40	65.08	63.15
TiO2	0.57	0.63	0.57	0.60	0.61	1.06	1.00	1.04	0.99
Al2O3	14.02	13.85	14.90	13.53	14.25	15.50	15.46	15.54	14.69
Fe2O3	3.15	3.60	3.32	3.57	3.30	6.72	5.71	4.60	6.03
MnO	0.04	0.09	0.02	0.09	0.04	0.14	0.10	0.11	0.10
MgO	0.62	0.66	0.67	0.78	0.45	2.19	3.27	1.90	1.83
CaO	2.20	2.15	2.60	2.30	2.97	5.96	5.25	2.65	5.00
K2O	5.62	5.19	4.88	5.69	5.37	3.69	3.10	3.86	4.47
Na2O	3.25	3.28	3.52	3.05	3.46	3.26	4.64	5.00	3.31
P2o5	0.15	0.11	0.15	0.13	0.14	0.43	0.35	0.11	0.33
Ba	387.24	497.9	22.84	223.23	250.21	180.01	318.11	246.38	10.39
Ce	721.10	500.22	292.64	389.43	564.20	535.50	636.50	468.39	353.37
Cs	1.00	1.22	0.99	1.10	0.98	0.97	1.00	1.20	1.00
Dy	56.40	48.61	31.39	43.79	37.49	52.17	34.22	31.10	24.08
Er	20.50	25.63	16.36	23.83	19.81	28.11	18.42	16.42	13.03
Eu	6.23	9.25	4.81	7.55	6.45	6.93	5.95	5.02	3.35
Gd	81.94	63.87	37.51	55.69	49.07	63.30	45.75	38.52	29.97
Ho	10.90	15.57	9.94	14.36	11.78	17.58	11.14	10.53	8.02
La	321.82	229.16	132.53	174.17	243.28	227.99	288.51	214.24	156.91
Lu	2.80	3.25	2.42	3.31	2.52	4.00	2.28	2.40	1.84
Nb	60.87	74.47	29.11	30.29	10.75	32.99	29.28	29.64	23.80
Nd	482.19	412.95	214.44	329.07	308.04	363.7	310.32	227.86	170.2
Pr	123.20	175.74	90.76	136.00	126.71	143.65	132.84	95.97	70.97
Rb	32.84	136.77	10.00	32.56	71.57	24.66	61.5	50.54	12.00
Sc	23.34	26.10	12.88	31.53	22.52	24.39	25.99	33.77	12.59
Sm	91.43	85.00	47.46	71.66	65.57	82.41	63.45	49.60	38.25
Sr	142.80	140.08	46.65	77.18	111.36	107.50	130.07	145.05	36.69
Ta	1.01	1.05	1.00	0.99	1.00	1.00	1.00	0.99	1.00
Tb	11.53	15.34	9.44	13.64	11.81	16.13	11.41	9.87	7.60
Th	39.00	27.86	30.65	25.81	22.48	39.14	23.86	24.14	21.40
Tm	0.99	1.20	0.90	1.19	0.90	1.48	0.90	0.90	0.90
U	35.40	36.07	12.44	26.74	15.03	17.46	12.11	19.36	6.26
Y	288.00	283.29	186.95	254.83	207.33	305.49	184.83	171.57	141.29
Yb	14.84	13.18	9.25	12.63	10.21	15.39	9.80	9.00	6.98
LOI	1.14	1.35	1.25	1.13	1.17	1.95	173	1.21	1.28

Table 5. Results of chemical analysis of granitoid mass concentrated samples. (Oxides are reported in wt. % and trace elements in ppm).

Samples	quartz monzodiorite		quartz monzonite	
	Const.1	Const.2	Const.3	Const.4
SiO2	63.62	64.73	64.50	64.30
TiO2	0.94	0.90	0.89	0.87
Al2O3	14.88	14.27	14.28	15.13
Fe2O3	6.00	5.87	6.02	3.89
MnO	0.12	0.06	0.07	0.09
MgO	2.00	1.45	1.47	2.00
CaO	4.81	3.61	3.69	4.52
K2O	3.50	5.77	5.72	5.88
Na2O	3.79	2.95	2.95	2.94
P2O5	0.26	0.32	0.33	0.32
Ba	63.10	274.55	270.04	353.13
Ce	234.76	607.64	218.2	391.85
Cs	1.10	0.90	0.89	0.99
Dy	39.47	35.86	26.08	20.86
Er	19.15	19.40	14.58	10.92
Eu	3.61	5.96	2.96	3.05
Gd	43.15	50.39	32.64	26.43
Ho	12.66	11.60	8.73	6.90
La	98.41	277.14	92.06	177.40
Lu	3.09	2.41	2.24	1.61
Nb	52.68	26.78	13.25	28.11
Nd	217.31	352.86	173.82	167.09
Pr	86.22	155.17	70.5	71.05
Rb	72.20	39.20	23.42	49.05
Sc	8.42	12.57	9.07	20.41
Sm	52.92	69.63	40.37	35.43
Sr	43.84	139.89	101.19	153.34
Ta	0.98	0.97	0.99	0.96
Tb	11.04	11.92	8.68	6.55
Th	31.27	33.46	29.49	18.7
Tm	1.14	0.90	0.90	0.90
U	8.37	21.22	7.08	15.84
Y	235.47	208.27	168.31	115.07
Yb	11.19	9.90	8.56	6.14
LOI	2.1	1.95	1.85	1.05
Sum	101.02	100.88	100.77	99.99

Microscopic studies were conducted to identify the minerals and, also to determine the degrees of liberation of the minerals by ZEISS Axioplan 2 polarizing light microscope with reflection and cross light. The mineralogical studies revealing that the major minerals contain quartz, apatite, calcite, magnetite and albite, the minor minerals (less than 10%) are phlogopite, zeolite,chlorite, hematite, pyrite, chalcopyrite, covellite, sphalerite, lepidocrocite, goethite, and monazite (Fig.4).

The milky to white and sometimes pink apatite crystallized as the main gangue mineral up to 20 cm in size in the magnetite ore, and is of the chlorine-fluorine-apatite type, and is seen as a hexagonal prism euhedralcrystal. Monazite crystals in Zanjan Iron oxide–apatite deposits are seen in three forms: euhedral shape in the intra-apatite inclusion with size 10 to 100 micrometers or hexagonal along the C axis, the boundary between apatite and magnetite crystals, subhedral in dimensions 20 to 150 µ., and inside the delayed carbonate veins they are seen euhedral with a size of 5 to 20 µ.

The degree of liberation of minerals was calculated by microscopic counting of particles, free and involved grains of minerals (Fig.-5 and table-6). Hematite is seen among fractures and low crystalline surfaces of magnetite, the highest involvement of magnetite in samples with hematite and then with non-metal gangues. Due to the high relationship between magnetite and hematite, it is difficult to calculate the degree of magnetite liberation. Mineral and ore interactions are mostly contact and less veinlet or inclusion, and are seen in three forms, including (magnetite-quartz-plagioclase), (magnetite-apatite-calcite) and (magnetite-pyrite-

plagioclase), and as the grain size decreases, the interactions are mostly binary especially (magnetite-apatite), (pyrite-magnetite), (plagioclase-magnetite) and (apatite-calcite). Table-4 shows the degree of liberation of apatite and magnetite-hematite, with decreasing dimensions, the degree of liberation of apatite increases. Accordingly, the dimensional fraction suitable for the release of apatite in the processing of the dimensional range is less than 75µ.

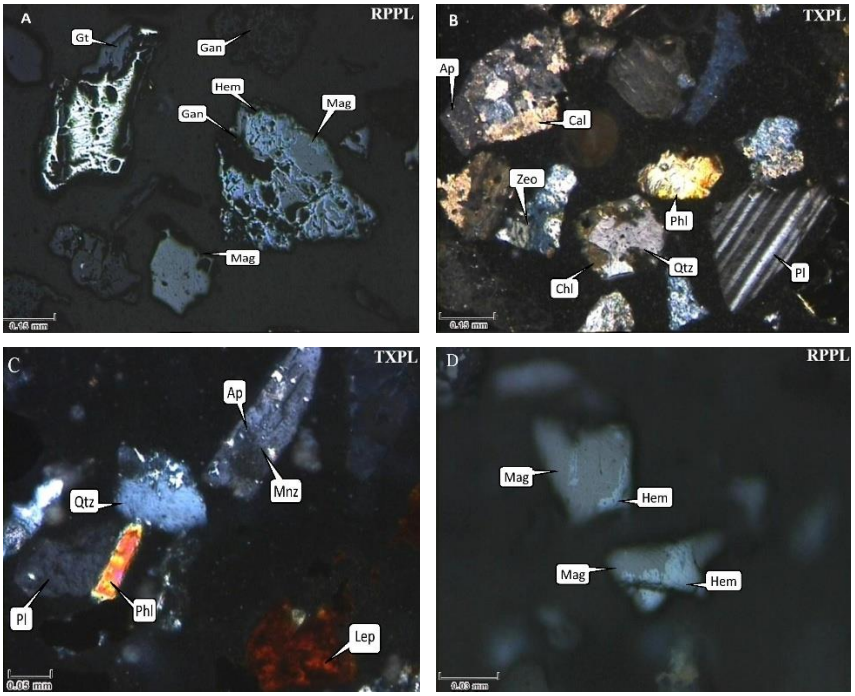

Fig 4. Petrography of samples at different scales (SEM-BSE images): (A) Magnetite and hematite are involved by gangue, pyrite is replaced by goethite (+150-300 µ); (B) photo micrograph of plagioclase, quartz, apatite, calcite, zeolite, phlogopite and chlorite (+150-300 µ). (C)Gangue minerals especially quartz, plagioclase, phlogopite, lepidocrocite, as well as monazite involvement in apatite (+75-150 µ) ; (D) Existence of free magnetite and hematite in Sample (≤75 µ). Magnetite(Mag); hematite(Hem); calcite(Cal); quartz(Qtz); phlogopite(Phl); gangue(Gan); plagioclase(Pl); apatite(Ap); zeolite(Zeo); monazite(Mnz); and lepidocrocite(Lep).

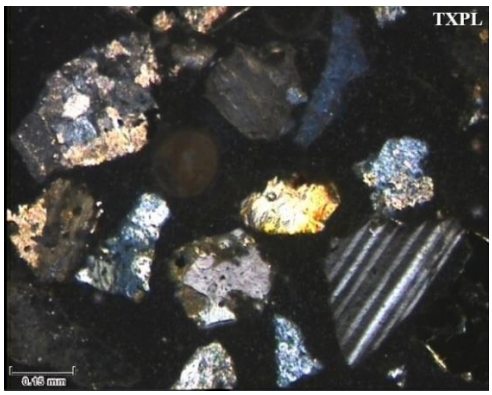

Fig 5. Apatite (Ap), calcite (Cal), magnetite (Mag), quartz (Qtz), phlogopite (Phl) and plagioclase (Pl)minerals as major minerals in dimensional range (d_{80} = 75µ)

Table 6. The degree of liberation of apatite and magnetite- hematite in different dimensional fractions

Magnetite- Hematite(%)	Apatite(%)	dimensional fractions(µ.)
56	55	-150 +300
72	75	-75 +150
85	82	-75

Based on the outcomes of the XRD analysis, the main minerals include plagioclase, quartz, magnetite, and apatite, and the sub-minerals zeolite, chlorite, phlogopite, and pyrite (Table 7). The results of the EPMA analyses are presented in the form of images from returned electrons (BSE) and EDS diagrams (Figs 6 , 7). Minerals containing REEs have a very high luminosity due to their higher density than the involved minerals and are marked with the abbreviation REE in the images. The main minerals containing REEs, in order of importance, include apatite, and magnetite. Minerals containing REEs ranges from 5 to more than 100 µ.

Table 7. Results of XRD analysis of iron oxide–apatite deposits in Morvarid Mine

Mineral Name	(wt %)	Mineral Name	(wt %)
Apatite (Ap)	10-15	Phlogopite (Phl)	3-7
Chalcopyrite (Ccp)	1-2	Sphalerite (Sp)	1>
Covellite (Cv)	1-2	Goethite (Gt)	2-4
Plagioclase (Pl)	30-35	Calcite (Cal)	2>
Pyrite (Py)	1-2	Chlorite (Chl)	2-4
Zeolite (Zeo)	2-4	Quartz (Qtz)	10-15
Monazite (Mnz)	1>	Magnetite (Mag)	30-40
Lepidocrocite (Lep)	2-4	Hematite (Hem)	2-4

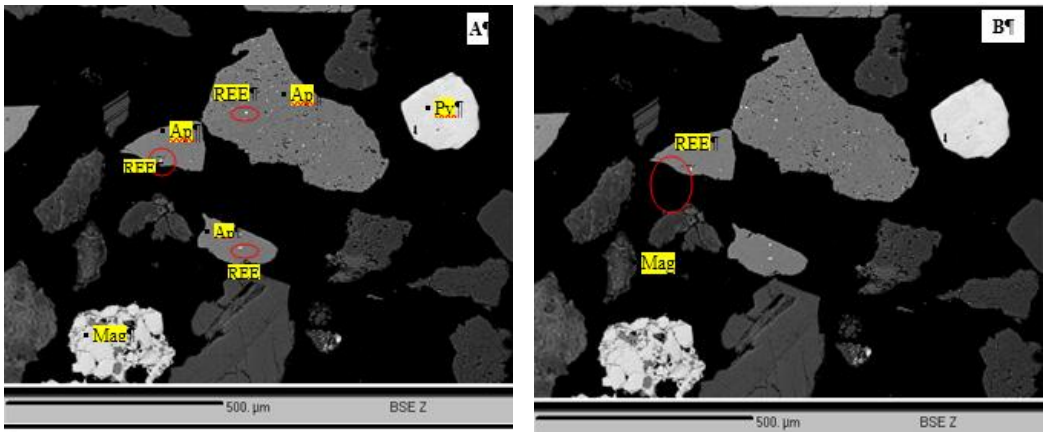

Fig 6. Petrography of samples at different scales (BSE images): (A) REEs in apatite in dimensional range (+150-300 µ), (B) REEs in magnetite in dimensional range (+150-300 µ): magnetite(Mag); apatite(Ap); pyrite(Py); and rare earth element(REE).

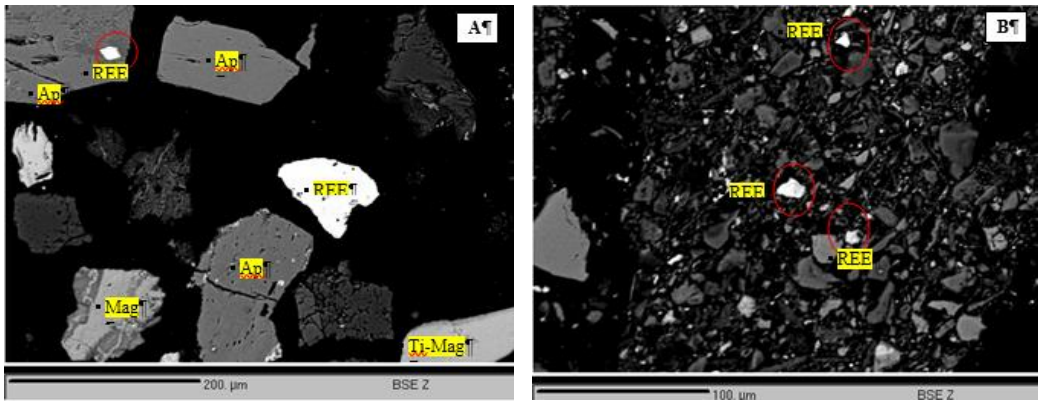

Fig 7. Petrography of samples at different scales (BSE images): (A) REEs within the apatite in dimensional range (+75-150 µ) micron (B): Free REEs in dimensional range (75-) µ. : magnetite (Mag); apatite(Ap); rare earth element(REE); and titano magnetite(Ti-Mag).

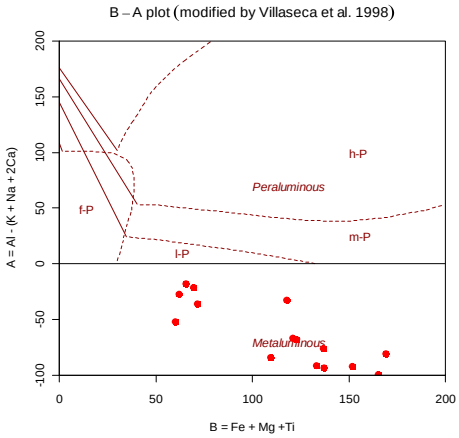

Fig 8. The type of the Tarom granitoid rocks on the Villaseca diagram (Villaseca et al. 1998).

4. Results and Discussion

4.1. Petrology and Geochemistry

The granitoid mass and ore samples were analyzed by ICP-MS method. Based on Chappell and white (1992) and Kanen (2001), the granitoids of study area, are I type. These rocks are Meta Aluminous (Fig.8) which are Characterized by A/CNK = $Al_2O_3/(CaO + Na_2O+K_2O) \leq 1$. According to Villaseca et al. (1998) the Meta Aluminous rocks consist of hornblende, biotite, pyroxene, magnetite, and ilmenite and Alkali feldspar minerals.

The variations of trace elements in granitoid rocks were compared with the concentrate and tailing samples. The study of the intrusive rocks in TAS and Middlemost diagrams, (Cox et al. 1979; Middlemost 1994) show that these rocks ranges from diorite, monzodiorite, to granodiorite, and the tailing range from granite to quartz diorite (granodiorite), monzonite, and quartz monzonite, and the concentrate comprises granodiorite and quartz monzonite (Figs. 9,10).In the diagram (Debon and Lefort 1988), the igneous rocks consist of the quartz diorite, tonalite, and quartz monzodiorite, the tailing are the quartz monzodiorite, and quartz monzonite, and the concentrate samples include quartz monzodiorite, and quartz syenite, (Fig 11).

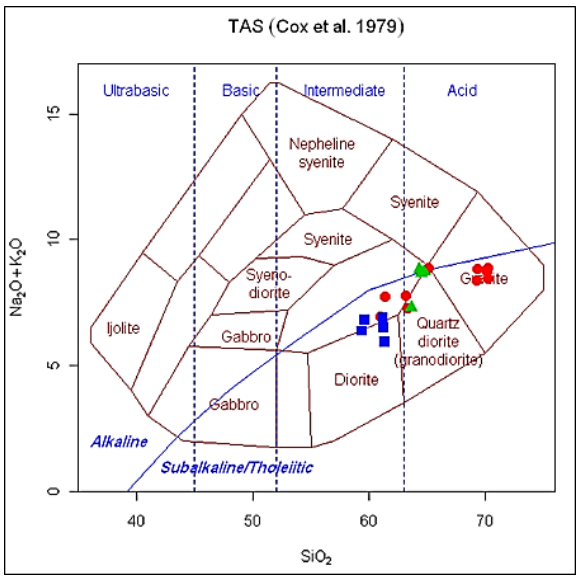

Fig 9. Classification of studied samples on the chart of Cox et al. 1979, the blue square is intrusive mass, red circle is tailing, and green triangle is concentrate.

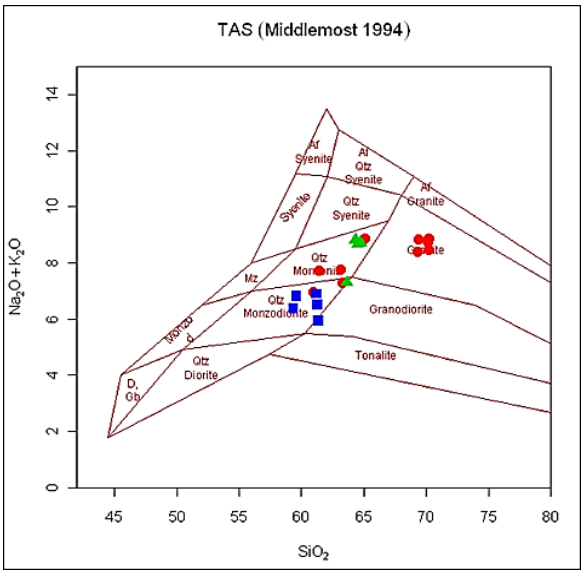

Fig 10. The position of the studied samples on the Middlemost (1994) chart, the blues squares are intrusion rock, the red circles are tailings and green triangles are concentrates.

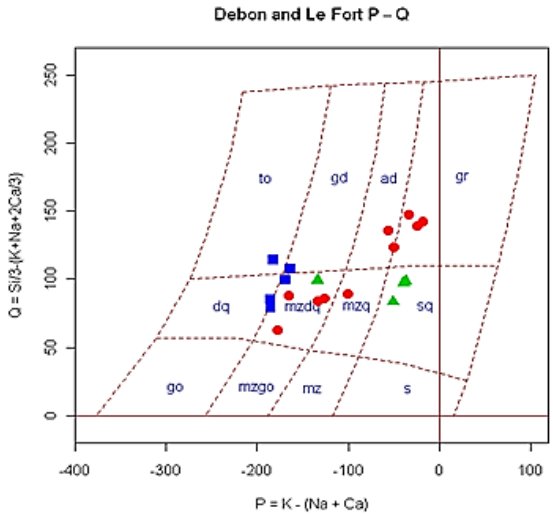

Fig 11. The position of the samples studied on the chart (Debon and Lefort 1988), the blue square is intrusive rocks, the red circle is tailing, and the green triangle is concentrate.

Based on the distribution of trace elements especially Nb, Rb, Ta, Y, Yb, and SiO_2 the granitoids were classified into four groups in terms of tectono magmatic position including: oceanic ridge granitoids (ORG), volcanic arc granitoids (VAG), within plate granitoids (WPG) and syn-collision granitoids (CCG) (Pearce et al. 1984). Several geologists such as Pearce et al. 1984; and Harris et al. 1984 have investigated the tectono magmatic position of granitoids in diagrams. According to the classification (Frost et al. 2001), the granites of the area are classified as orogeny type (I and S) granites, (Fig.12).According to Azizi et al. 2009, the ratio of alkaline elements in Morvarid granites include high K/Rb (K/Rb>100) and low Rb/Sr (Rb/Sr<10) indicating I-type granite.The tectono-magmatic setting of rocks has been studied based on chemical composition of LREEs. Generally, four graphs plotted based on Y/Yb, Rb/Yb + Nb, Yb/Ta, Rb/Yb + Nb to differentiate tectono-magmatic setting of granitoids. Pearce, 1996 developed his earlier graphs and finally concluded that this granitoid were determined the range of Post-COLG in place for Syn-COLG, WPG, and in the range of volcanic arc granitoid (VAG) (Fig 13).Based on diagrams obtained from normalization of granitoid mass with chondrite data (Sun and McDonough 1989) (Fig 14), samples, enrichment of LREE such as Ce, La, and Pr, relative to HREE including Lu, Tm, and Yb. Negative anomaly of Eu not only indicates oxidation and reduction conditions in magma, but also indicates entry of divalent element into feldspar structure especially plagioclases, in other words, plagioclase crystal dissociation in magma can cause anomaly has been, In the said processes, Pr as a mobile element, depicting comparatively high concentration. So the Tarom'sgranitoid are (VAG), and collision granitoids (VAG + syn + COLG). The granitoids are calc-alkaline, high K and meta-aluminous range, revealing a post-collision tectonic environment and the subduction setting.

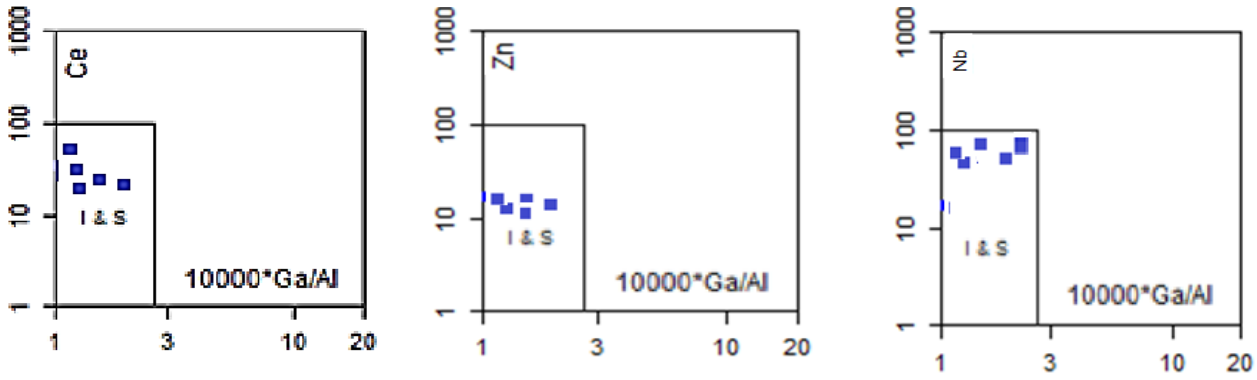

Fig.12. Ce, Zn and Nb vs. 10000 * Ga/Al discrimination diagrams of Frost et al, 2001. I and S type granites.

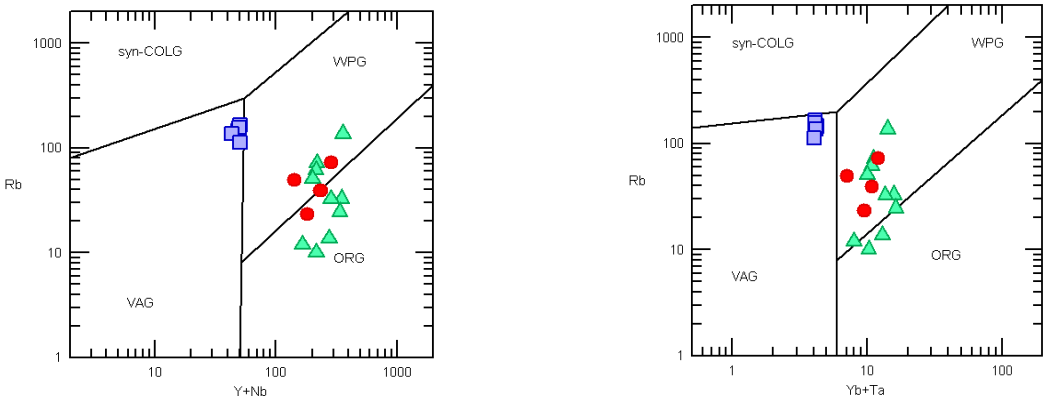

Fig 13. The tectono magmatic setting of the studied samples on the Pearce et al. 1984 and Pearce.1996 chart, the blue square is intrusive rock, the red circle is tailing, and green triangle is concentrate.

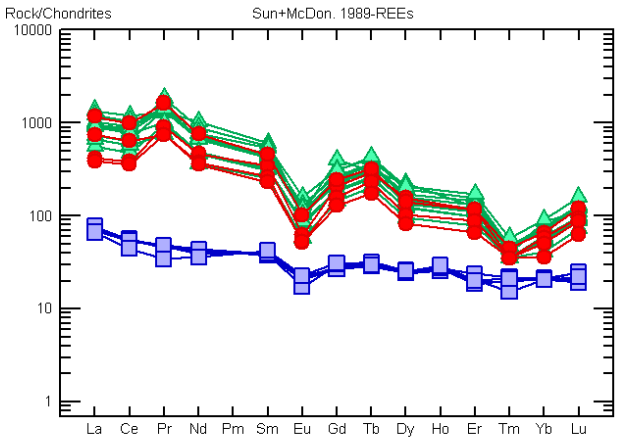

Fig 14. Normalized pattern of granitoids rocks (blue square), tailing (red circle), and concentrated samples (green triangle) (Sun and McDonough, 1989).

4.2. The Acid Leaching and Digestion process

Distilled water was used to carry out the basic leaching experiments and the ranges of 0.1–12.0 M for sulfuric acid and 0.5–3.0 M for hydrochloric distilled water were simulated three time. Furthermore, the achieved average values were applied to do the analysis. An aluminum foil was used to keep temperature constant and to avoid evaporation. A certain volume of distilled water was added when the amount of the pulp is reduced. At consistent time interludes , the solution samples were joined together and by means of a filter for lower acid conditions (0.1–2.0 M acids) or a centrifuge for higher acid conditions (5.0–13.0 M acids), the solid particles were separated from the leachate(Adib et al. 2021b). The solution diluted with 1.0 M hydrochloric acid to avoid precipitation of REEs and consequently was analyzed.

4.2.1. The Acid leaching Experiments

By dint of sulfuric acid digestion process the apatite concentrate is treated. The resulted cake is washed using distilled water. To determine the optimal conditions, apatite concentrate was added to the heating sulfuric acid, stirrer for a certain period of time. Finally a dry gray solid residue was obtained. Subsequently, the digested mass was leached once again by distilled water. For leaching, a discontinuous Pyrex reactor with a hot plate was used, the suspension sample was stirred with a magnetic stirrer at a certain temperature. The specified value of the material produced in the digestion stage was added to distilled water. Next, a centrifuge was used to filter the leach liquor and the precipitate were analyzed by means of IC-Mass. The leaching process in various sulfuric acid concentration, at one hour time and the temperature of 25^0Cis displayed in Fig 15.

At low acid concentrations, the leaching recovery increased with increasing acid concentration. Consequently, the leaching level decreases towards 4.0 M. The re-precipitation of REEs through the formation of calcium sulfate is the main caused of this reduction.

Obviously, when calcium and sulfate are both present in aqueous solution (El-Nadi et al. 2013; Adib et al. 2021b), gypsum, hemihydrate, and anhydrite are formed. With the use of the XRD analyses, the presence of CaSO4·2H2O and CaSO4 are confirmed in the residue after leaching, as shown in Fig 16. Since the ionic radius of Ca and REEs are similar, the residue might comprise REEs through substituting isomorphs for Ca2+ (Azimi and Papangelakis 2010). Fig 17 illustrates the differences in the leaching recovery at the diverse times. At 12.0 M sulfuric acid, with increasing the leaching time from 1 to 4 hours the recovery increases with a high slope. The equilibrium of the leaching reaction is happen by extending the time to 6 hours. Although with sulfuric acid concentrations of 12M and leaching time of 6 hours, the significant recovery has not been attained. The highest recovery is for La with about 62 percent. Meanwhile, the total soluble Ca compound differs as the result of the sulfuric acid concentration in a pattern is like the leaching form. According to this result, it is concluded that sulfuric acid may not be an appropriate leaching agent for this ore. Further, Ca (REE) sulfate precipitation can be a side reaction, restraining the REE leaching recovery, as did not exceed 62%, although at concentration of acid 12.0M, and time leaching of 6 h. Furthermore, a very high concentration of high soluble Ca types, would certainly subjects to hitches throughout REE recovery using either solvent extraction or precipitation. The difference in the leaching recovery with the primary concentration of hydrochloric acid is presented in Fig 18. When the concentration was lower than 1.0 M, any of the REEs were not leached. The leaching recovery remarkably improved when the concentrations of hydrochloric acid were greater Approximately 90% of the REEs were leached at an acid concentration of 3.0M,. Nonetheless, there was plenty of Ca in the leachate.

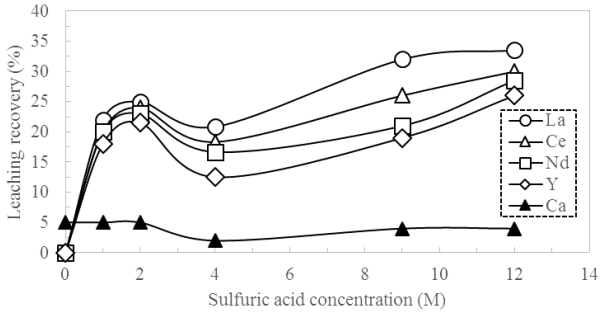

Fig 15. Leaching recovery at various initial sulfuric acid concentrations at 25°C, Leaching time: 1 h

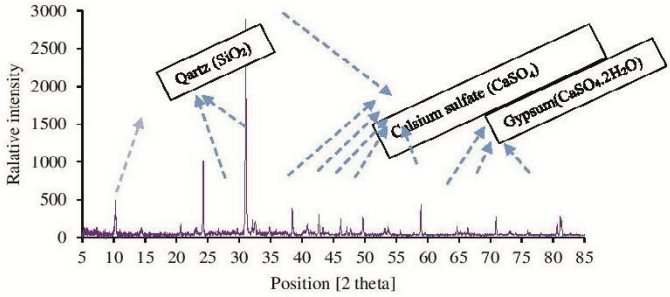

Fig 16. XRD analysis of residue from leaching with sulfuric acid.

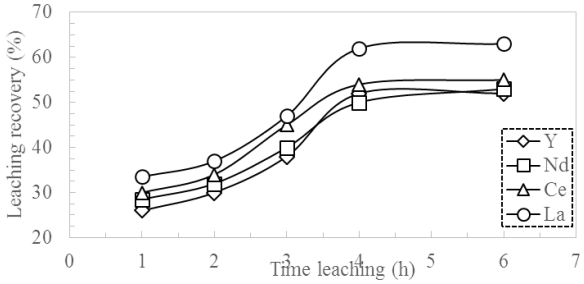

Fig 17. Change leaching recovery with time, using sulfuric acid at 25°C, acid concentration 12.0M and L/S ratio: 5:1

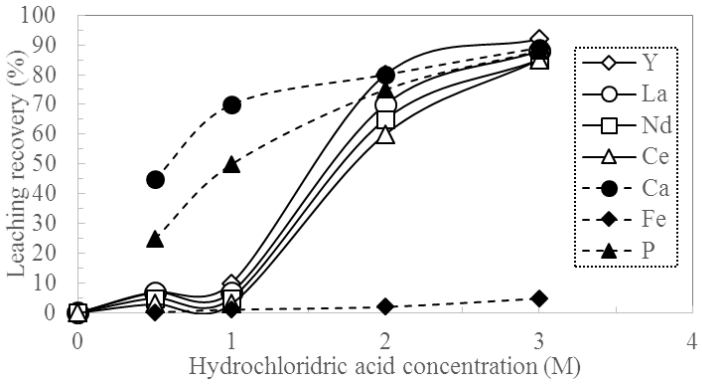

Fig 18. Changes in Leaching recovery at different concentrations of sulfuric acid at 25°C, Leaching time: 2.5 hours and L/S ratio: 5:1

Fig 19 features out the differences in the leaching recovery with distinct concentrations of Nitic acid impurities such as P and Ca were properly leached, while no REEs, aside from Y, were leached at 1 M. Nevertheless, round 90% of the REEs were leached, once the acid concentration was greater to 3.0 M. The outcomes of these investigates are the same as those of the hydrochloric acid. Nitric acid was not deliberated in later tests since hydrochloric acid is comparatively chipper. Hence, for apatite REE ore, hydrochloric acid was selected as the leaching media.

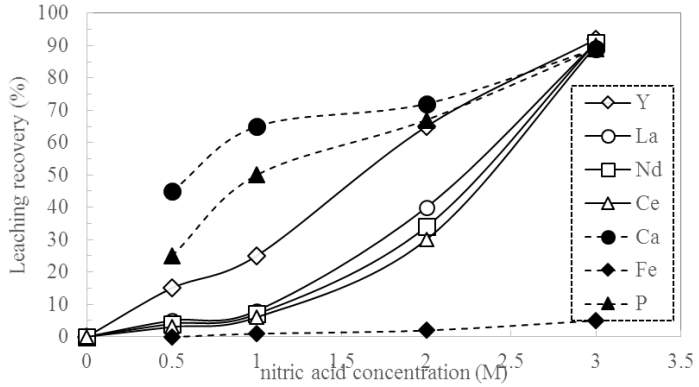

Fig 19. Leaching recovery at several nitric acid concentrations at 25°C, Leaching time: 2.5 h, L/S ratio: 5:1).

4.2.2. Digestion process

The outcome of digestion temperature on the recovery of REEs from apatite with persistent conditions of 3 hours and S/L ratio of 1.75 is displayed in Fig 20. The acidic digestion process, contributes to break the strong bindings and form soluble REEs' sulfates. The reactions in digestion procedure are: (Wang et al. 2010).

The outcome of digestion temperature on the recovery of REEs from apatite with persistent conditions of 3 hours and S/L ratio of 1.75 is displayed in Fig 20. The acidic digestion process, contributes to break the strong bindings and form soluble REEs' sulfates. The reactions in digestion procedure are: (Wang et al. 2010).

$$2REPO_4\,(s) + 3H_2SO_4 \rightarrow (RE)_2(SO_4)_3\,(s) + 6H^+ + 2PO_4^{3-} \quad (1)$$

$$Th_3(PO_4)_4\,(s) + 6H_2SO_4 \rightarrow 3Th(SO_4)_2\,(s) + 12H^+ + 4PO_4^{3-} \quad (2)$$

$$ThSiO_4 + 2H_2SO_4 \rightarrow Th(SO4)_2 + SiO_2 + 2H_2O \quad (3)$$

$$Ce3(PO_4)_4(s) + 6H_2SO4 \rightarrow 3Ce(SO_4)_2(s) + 12H^+ + 4PO_4^{3-} \quad (4)$$

The outcomes indicated that temperature does no significantly affect the digestion due to the following reasons. As shown in Fig 20, the low recovery of the digestion process is caused by the temperature increases due to several reasons. The first reason is attributed to the accumulation of the compounds which are insoluble. Another reason is that the rate of the sulfuric acid evaporation is increased since the digestion stage is not done in the vacuum and the system is affected by the air (Gupta 1990). Consequently, reducing the reaction time between solid and liquid.

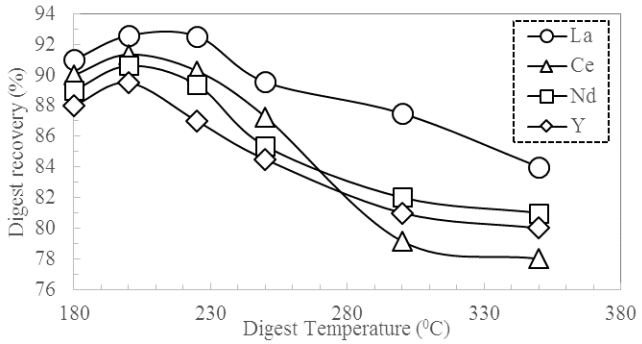

Fig 20. The outcome of digestion temperature on the recovery of the REEs from apatite with of 3 hours time and S/L ratio of 1.75.

The fallouts of the recovery of the REE with conditions of 220 °C and 3 hours in a diverse L/S are presented in Fig 21. Consequently, the recovery of REE minerals up to 90% is as the result of enhancing the L/S ratio from 0.5 to 2. The recovery remains almost constsnt when the L/S ratio is more than 2. Increasing the L/S ratio subjects to develop the recovery of the REE on account of the probability of operational contacts between the solid and liquid. It is suggested that the ideal state in the digestion is obtained at the temperature of 220°C, time of 3 hours, and the L/S ratio of 2.0.

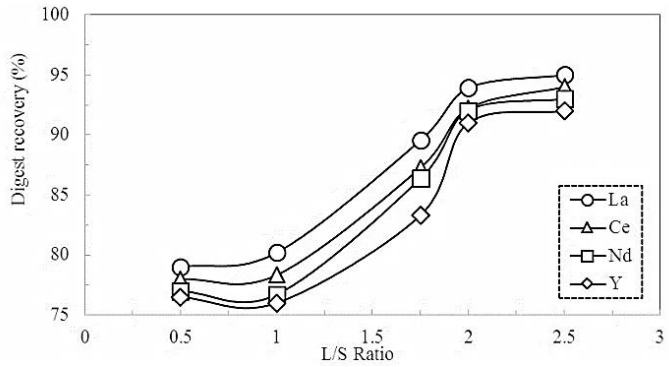

Fig 21. Effect of the L/ S ratio on the recovery of REEs in digestion at 220 °C for 3 hours.

4.2.3. Aqueous Leaching

In fact, sulfate salts of REEs and REES sulfates are mostly included in the dry gray digested mass, dissolved in distilled water. Some impurities contains, unreacted appetites and insoluble compounds made in the digestion process are left as sediments. In the leaching stages, the subsequent reactions are: (Wang et al. 2010).

$(RE)_2(SO_4)_3.nH_2O(s) \rightarrow 2RE_3+ +3SO_4^{2-} +nH_2O$ (5)

$Th(SO_4)_2(s) \rightarrow Th_4+ +2SO_4^{2-}$ (6)

$(SO_4)_2\ (s) \rightarrow Ce_4+ +2SO_4^{2-}$ (7)

However, researches on the digestion and leaching step are not in unit agreement.

The outcome of aqueous leaching time on leaching with L/S=5 and 25°C is displayed in Fig 22. Within 5 h, the recovery of 55.5, 54. 5, 58.2 and 60% were recorded as the highest for La, Ce, Nd, and Y, correspondingly. Noticeably, the uppermost rate of recovery of REES for La, Ce, Nd, and Y was 84.0, 83.5, 54.3 and 86.0%, at 80 °C, individually. The effect of water leaching temperature on leaching recovery with perpetual conditions L/S = 5 and time of 5 hours is illustrated in Fig 23. Evidently, the upperrmost ate of recovery of REES for La, Ce, Nd, and Y was 84.0, 83.5, 54.4 and 86.0%, at 80 °C, individually.The result of changes in L/S ratio on leaching recovery in 5 hours and temperature of 80°C is displayed in Fig 24. The recovery of 89.5, 88. 5, 92.2 and 94.0% correspondingly at L/S = 10 are the utmost obtained rate for La, Ce, Nd, and Y. The increment of the L/S ratio leads to increase the recovery of the REEs. This is due to the fact that the interfaces of liquid and solid are enhanced. This is exactly where it is expected to detect the reaction between solid and liquid.) Also, increasing the L/S ratio causes the solution to become saturated later, and these all increase the leaching recovery (Hu and Qi 2014; Kumari et al. 2014). As the optimum water leaching conditions are 5 h time and 80 °C and L/S of 10, the uppermost recovery of REEs from digest solid for La, Ce, Nd and Y 89.5, 88. 5, 92.2 and 94.0% were achieved, correspondingly.

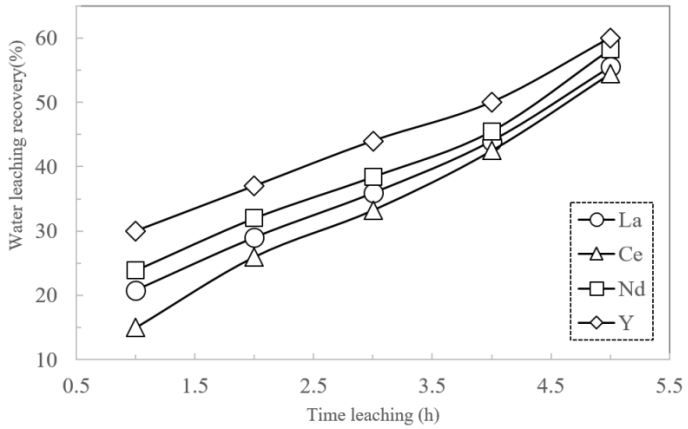

Fig 22. Influence of water leaching time on recovery with known conditions L/S = 5 and 25 °C

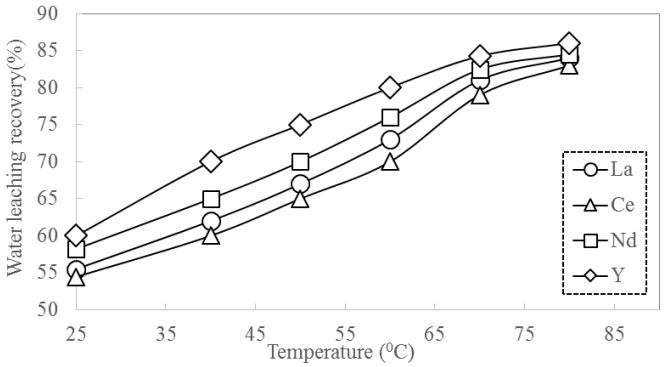

Fig 23. Effect of aqueous leaching temperature on leaching recovery with constant conditions L/S = 5 and leaching time of 5 hours.

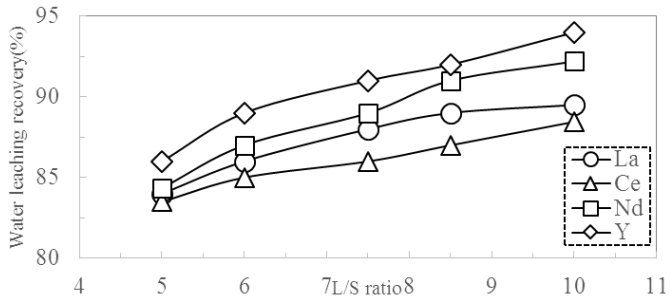

Fig 24. Influence of L/S ratio on the recovery of water leaching with persistent settings of 80 °C and 5 hours.

5. Conclusions

Based on the petrology, diorite, monzodiorite, quartz monzodiorite, monzonite, granodiorite, and quartz syenite are the main intrusive rocks of the Sorkheh-Dizaj Mines. Elements such as Ce La, Nd, and Y present in monazitelattice and in the magnetite ore are found. Granitoid rocks are classified as arc and collision granitoids (VAG + COLG).) Based on chondrite normalized REEs of Taromgranitoide rocks, the enrichment of LREEs such as La, Ce, Pr and HREEs comprises of Tm, Yb and Lu. Taromgranitoids are calc-alkaline, high K and meta-aluminous range, and showed a post-collision tectonic environment. The negative trend from LREEs to HREEs is consistent with the spider pattern of the subduction areas. The outcomes of the ICP analysis indicated that4.86% REEs (La, Ce, Y and Nd) is included in the apatite concentrate.

According to the sulfuric acid leaching experiments, it is determined that increasing the acid concentration up to 2

M subjects to enhance the recovery of the REES. REEs that consequently increase the acid concentration up to 4 M and hence reduce the recovery. Evidently, when the conditions are optimum in sulfuric acid, the uppermost recovery of REEs is roughly 62%. In a digestion test with sulfuric acid at temperature of 220° C, , time of 3 hours and ratio of L/S of 2.0, and 3M acid sulfuric, the obtained recovery of REEs (La, Ce, Nd and Y) was 92.92, 92.22, 92.04% and 91.00%, respectively.

The leaching investigation carried out by hydrochloric and nitric acids, it is revealed that with optimum conditions of 25° C, 2.5 hours, L/S ratio of 5: 1 , the achieved recovery of the Ce, La, Nd, and Y is of nearly 90%. The results also showed the aqueous leaching in digestion process, with 5 h time, 80° C and L/solid ratio of 10, the highest recovery of La, Ce, Nd, and Y was 89.5%, 88. 5%, 92.2%, and 94.0%,. The water leaching experiments show that the uppermost recovery of La, Ce, Nd, and Y was 89.5%, 88. 5%, 92.2%, and 94.0% respectively, which is achieved at 5 h time, 80° C and L/S ratio of 10.

Acknowledgments

This article is extracted from the results of a research project and therefore the authors are grateful for the support of Islamic Azad University, South Tehran branch.

References

Adib A, Ahmadi R, Rahimi E (2021b) The Recovery of Rare-Earth Elements from Apatite concentrate by Acid and Digestion-Water Leaching Processes in Morvarid iron Mine, Iran. *Journal of Mining Science 57:131-43*.

Adib A, Nabilou M, Afzal P (2021a) Relationship between Fe-Cu-REEs mineralization and magnetic basement faults using multifractal modeling in Tarom region, NW Iran. *Episodes Episodes Journal of International Geoscience 1;45(3):223-37*.

Aly MM, Mohammed NA (1999) Recovery of lanthanides from Abu Tartur phosphate rock, Egypt. *Hydrometallurgy 52: 199–206.*

Azimi G, Papangelakis VG (2010) The Solubility of gypsum and anhydrite in simulated laterite pressure acid leach solutions up to 250″C. *Hydrometallurgy 102: 1–13.*

Azizi H, Mehrabi B and Akbarpour A (2009) Genesis of Tertiary Magnetite–Apatite Deposits, Southeast of Zanjan, Iran, *Resource Geology 59(4):330-41*.

Baratian M, Arian MA, Yazdi A (2018) Petrology and petrogenesis of the SiahKuh intrusive Massive in the South of KhoshYeilagh, *Amazonia Investiga* 7 (17): 616-629.

Chappell BW, White AJR (1992) I- and S-type granites in the Lachlan Fold Belt. Transactions of the Royal Society of Edinburgh, *Earth Sciences 83: 1-26*.

Chi R, Tian J, Zhu G, Wu Y, Li S, Wang C, Zhou ZA (2006) Kinetics of rare earth leaching from a manganese-removed weathered rare-earth mud in hydrochloric acid solutions. *Separation Science and Technology 41: 1099–1113*.

Cox KG, Bell JD, Pankhurst RJ (1979) the interpretation of igneous rocks. George, Allen and Unwin, London.

Davoudian AR, Genser J, Dachs E, Shabanian N (2008) Petrology of eclogites from north of Shahrekord, Sanandaj-Sirjan zone, Iran. *Mineralogy and Petrology 92: 393-413*.

Debon F, Le Fort P (1988) A cationic classification of common plutonic rocks and their magmatic associations: principles, method, applications. *Bulletin de Minéralogie 111: 493–510*.

El-Nadi Y, El-Hefny NE, Aly HF (2013) Solvent extraction and recovery of Y(III) and Yb(III) from fluorspar mineral. Internarial journal of minerals, *Metallurgy and Materials 20: 713-719*.

Frost, B. R., Barnes, C. G., Collins, W. J., Arculus, R. J., Ellis, D. J. & Frost, C. D. (2001). A geochemical classification for granitic rocks. *Journal of Petrology 42: 2033–2048*.

Gharib-Gorgani F, Ashja-Ardalan A, Espahbod MR, Sheikhzakariaee SJ, Yazdi A (2017) Petrology of Mg-bearing Meta Ophiolite Complexes of Qaen-Gazik, Eastern Iran, *National Cave Research and Protection Organization* 4(1): 1-6.

Ghasemi A, Talbot CJ (2006) A new tectonic scenario for the Sanandaj-Sirjan Zone (Iran). *Journal of Asian Earth Sciences 26: 683-693*.

Golonka J (2004) Plate tectonic evolution of the southern margin of Eurasia in the Mesozoic and Cenozoic. *Tectonophysics 381: 235-273*.

Gupta CK (1990) Hydrometallurgy in Extraction processes, Wiley-VCH.

Gupta CK, Krishnamurthy N.(2005) Extractive Metallurgy of Rare Earths, CRC, Press, Florida.

Hassanzadeh J, Ghazi AM, Axen G, Guest B (2002) Oligomiocene mafic-alkaline magmatism north and northwest of Iran: evidence for the separation of the Alborz from the Urumieh–Dokhtar magmatic arc. *Geological Society of America Abstracts with Programs 34: 331*.

Henderson P (1984) Rare earth element geochemistry. Developments in geochemistry, 2. Elsevier, Amsterdam.

Hu Z, Qi L (2014) Sample Digestion Methods, *Elsevier Ltd: 87-109*.

Jones AP, Wall F, Williams CT (1996) Rare earth minerals-chemistry, origin and ore deposits; Chapman & Hall: London, UK.

Jorjani E, Bagherieh AH, Chelgani SC (2011) Rare earth elements leaching from Chadormalu apatite concentrate: Laboratory studies and regression predictions. *Korean Journal of Chemical Engineering. 28: 557–562.*

Kanen R (2001) Distinguishing between S and I type granites. Minerals Services, Melbourne, Australia.

Kim E, .Osseo-Asare K (2012) "Aqueous stability of thorium and rare earth metals in monazite

hydrometallurgy: Eh–pH diagrams for the systems Th– , Ce–, La–, Nd– (PO4)–(SO4)–H2O at 25 C" *Hydrometallurgy 113–114: 67-78.*

Kim E, Bae I, Chai S, Shin H (2009) Mechano-chemical decomposition of monazite to assist the extraction of rare earth elements, *Journal of Alloys and compounds 3;486(1-2):610-4.*

Kim E, Osseo-Asare K (2012) Aqueous stability of thorium and rare earth metals in monazite hydrometallurgy: Eh–pH diagrams for the systems Th– , Ce–, La–, Nd– (PO4)–(SO4)–H2O at 25 C, *Hydrometallurgy 113–114: 67-78.*

Kim R, Cho H, Han KN, Kim K, Mun M (2016) Optimization of acid leaching of rare earth elements from Mongolian Apatite-Based Ore *Minerals 30;6(3):63.*

Kumari A, Panda R, Jha MK, Lee JY, Kumar JR, Kumar V (2014) Thermal treatment for the separation of phosphate and recovery of rare earth metals (REMs) from Korean monazite, *Journal of Industrial and Engineering Chemistry 21: 696-703*.

Middlemost EAK (1994) Magmas and magmatic rocks, an introduction to igneous petrology, Longman, London.

Mokhtari MAA, Sadeghi M, NabatianGh (2018) Geochemistry and potential resource of rare earth element in the IOA deposits of Tarom area, NW Iran. *Journal of Ore Geology Reviews 92:529–541*.

NabatianGh, Ghaderi M (2013) Oxygen isotope and fluid inclusion study of the Sorkhe- Dizaj iron oxide-apatite deposit, NW Iran. International Geology *Review 55(4): 397-410.*

NabatianGh, Ghaderi M (2014) Mineralogy and geochemistry of rare earth elements in iron oxide-apatite deposits of the Zanjan region. Scientific Quarterly Journal of Geosciences, Geological *Survey and Mineral Exploration of Iran 24:157–170*.

NabatianGh, Li XH, Honarmand M, Melgarejo JC (2017) Geology, mineralogy and evolution of iron skarn deposits in the Zanjan district, NW Iran: Constraints from U-Pb dating, Hf and O isotope analyses of zircons and stable isotope geochemistry. *Ore Geology Reviews 84:42–66*.

Pearce JA (1996) Sources and setting of granitic rocks. *Episodes 19(4):120-5.*

Pearce JA, Harris NBW, Tindle AG (1984) Trace element discrimination diagrams for the tectonic interpretation of granitic rocks. *Journal of Petrology 25: 956 – 983.*

Pereira F, Bilal E (2016) Phosphoric acid extraction and rare earth recovery from apatites of the Brazilian phosphates ores. *Romanian journal of Mineral Deposits 85(2):49-52.*

Preston JS, Cole PM, Craig WM, Feather AM (1996) the recovery of rare earth oxides from a phosphoric acid by product. Part 1: Leaching of rare earth values and recovery of a mixed rare earth oxide by solvent extraction Hydrometallurgy *41(1):1-9.*

Sandström A, Fredriksson A (2012) Apatite for extraction leaching of Kiirunavaaraapatite for simultaneous production of fertilizers and REE. In Proceedings of the 26th International Mineral Processing Congress, IMPC 2012: Innovative Processing for Sustainable Growth, New Delhi, India, 24–28: 4707–4714.

Sarem MN, Abedini MV, Dabiri R, Ansari MR. (2021) Geochemistry and petrogenesis of basic Paleogene volcanic rocks in Alamut region, Alborz mountain, north of Iran. *Earth Sciences Research Journal* 25(2): 237-245.

Şengör AMC, Nataln'in BA (1996) Paleotectonics of Asia: Fragments of a synthesis, In: Yin AM, Harrison T (eds.), The Tectonic Evolution of Asia. *Cambridge University Press*: 486-640.

Stockli DF, Hassanzadeh J, Stockli LD, Axen G, Walker JD, Dewane TJ (2004) Structural and geochronological evidence for Oligo-Miocene intra-arc low angle detachment faulting in the Takab-Zanjan area, NW Iran. Abstract, *Programs Geological Society of America* 36: 319.

Sun SS, Mc Donough WF (1989) Chemical and isotopic systematics of ocean basalts: implications for mantle composition and processes. In: Saunders A D, and Norry, M J. (Eds.), Magmatism in the ocean basins. Geological Society of London, Special Publication, 42. Black Well, *Oxford*,:313 – 346.

Thirlwall, M. F., Smith, T. E., Graham, A. M., Theodorou, N., Hollings, P., Davidson, J. P. and Arculus, R. J. (1994) High field strength elements anomalies in arc lava: source or process? *Journal of petrology 1;35(3):819-38.*

Villaseca C, Barbero L, Herreros V (1998) A re-examination of the typology of peraluminous granite types in intracontinental orogenic belts. *Earth and Environmental Science Transactions of the Royal Society of Edinburgh 89: 113–119*

Wang L, Long Z, Huang X, Yu Y, Cui D, Zhang G (2010) Recovery of rare earths from wet-process phosphoric acid. *Hydrometallurgy 101: 41–47*.

Yazdi A, Shahhosseini E, Moharami F (2022) Petrology and tectono-magmatic environment of the volcanic rocks of West Torud–Iran, *Iranian Journal of Earth Sciences* 14 (1): 40-57.

Yazdi A, Ziaaldini S, Dabiri R (2015) Investigation on the Geochemical Distribution of REE and Heavy Metals in Western Part of Jalal-Abad Iron Ore Deposit, Zarand, SE of Iran, *Open journal of ecology* 5 (09): 460-476.